Evidence for Preorganization of the *glmS* Ribozyme Ligand Binding Pocket†

Ken J. Hampel* and Melissa M. Tinsley

Department of Microbiology and Molecular Genetics, University of Vermont, 95 Carrigan Drive, 222 Stafford Hall, Burlington, Vermont 05405

Received February 17, 2006; Revised Manuscript Received April 21, 2006

ABSTRACT: We have examined the tertiary structure of the ligand-activated *glmS* ribozyme by a combination of methods with the aim of evaluating the magnitude of RNA conformational change induced by binding of the cofactor, glucosamine 6-phosphate (GlcN6P). Hydroxyl radical footprinting of a trans-acting ribozyme complex identifies several sites of solvent protection upon incubation of the RNA in Mg^{2+}-containing solutions, providing initial evidence of the tertiary fold of the ribozyme. Under these folding conditions and at GlcN6P concentrations that saturate the ligand-induced cleavage reaction, we do not observe changes to this pattern. Cross-linking with short-wave UV light of the complex yielded similar overall results. In addition, ribozyme−substrate complexes cross-linked in the absence of GlcN6P could be gel purified and then activated in the presence of ligand. One of these active cross-linked species links the base immediately 3′ of the cleavage site to a highly conserved region of the ribozyme core and could be catalytically activated by ligand. Combined with recent studies that argue that GlcN6P acts as a coenzyme in the reaction, our data point to a riboswitch mechanism in which ligand binds to a prefolded active site pocket and assists in catalysis via a direct participation in the reaction chemistry, the local influence on the geometry of the active site constituents, or a combination of both mechanisms. This mode of action is different from that observed for other riboswitches characterized to date, which act by inducing secondary and tertiary structure changes.

Riboswitches are mRNA elements that control expression of a large number of bacterial and some eukaryotic genes (*1*−*6*). Found predominantly in the 5′-untranslated regions of mRNAs, these RNA motifs bind small molecules, often the products of the enzymes encoded by their mRNAs. Riboswitch RNAs adopt a stable conformation in the absence of ligand, but ligand binding by the RNA induces a conformational switch to an alternative structure that acts directly to modulate gene expression (*1*). These conformational changes generally entail a secondary structure rearrangement that induces transcriptional termination or inhibits ribosome binding by sequestering the Shine-Delgarno sequence of the mRNA. A third strategy was recently identified in a riboswitch that responds to glucosamine 6-phosphate (GlcN6P)[1] binding by cleaving a target site upstream of the start codon for the *glmS* gene (*7*). The product encoded by the *glmS* gene, glutamine-fructose-6-phosphate amidotransferase, generates GlcN6P and glutamate from fructose 6-phosphate and glutamine. Though a highly conserved consensus sequence is available for the *glmS* RNA motif from Gram-positive bacteria, there is insufficient evidence to conclude that changes in tertiary or secondary structure are induced by ligand binding (*2*, *7*). In principle, only local structural rearrangement is required to activate catalysis by a small molecule-dependent ribozyme. For example, group I introns are activated by binding of the substrate guanosine, the nucleophile in the first step of splicing, and the Mg^{2+} ions that are required to catalyze the reaction (*8*). Nevertheless, folding of group I introns into an active conformation in the presence of Mg^{2+} can be accomplished in the absence of guanosine in cases where water serves as the nucleophile (*9*, *10*). The *glmS* ribozyme may similarly preorganize a binding pocket for GlcN6P. Supporting this hypothesis are recent data from the Soukup laboratories that provide evidence for the direct participation of the sugar amine of GlcN6P in the cleavage reaction (*11*).

A secondary structure has been proposed for the catalytic motif on the basis of phylogenetic variation between several Gram-positive bacteria (*2*). The motif contains four major stem−loop structures, P1−P4, two of which contain conserved internal loops (P2 and P4) (Figure 1). The internal loop between P2 and P2a is highly conserved, and its 3′-half is proposed to form an important pseudoknot, P2.1, with the single-stranded sequence immediately downstream of the cleavage site (*12*). A second pseudoknot, P3.1, has been shown to form between L3 and the sequences 3′ to P4 and though nonessential for catalysis promotes higher levels of cleavage activity and reduces the Mg^{2+} requirement for the cleavage reaction (*13*, *14*).

The chemical mechanism of site-specific self-cleavage appears to be similar to that observed in many small natural

† This work is supported by Grant AI44186 to Dr. J. M. Burke from the National Institutes of Health.

* To whom correspondence should be addressed: Department of Microbiology and Molecular Genetics, University of Vermont, 95 Carrigan Dr., 222 Stafford Hall, Burlington, VT 05401. Telephone: (802) 656-8507. Fax: (802) 656-8749. E-mail: khampel@uvm.edu.

[1] Abbreviations: EDTA, ethylenediaminetetraacetic acid; GlcN6P, glucosamine 6-phosphate; HPLC, high-performance liquid chromatography; mRNA, messenger ribonucleic acid; PAGE, polyacrylamide gel electrophoresis; PCR, polymerase chain reaction; Tris, tris(hydroxymethyl)aminomethane; tRNA, transfer ribonucleic acid; UV, ultraviolet; VS, Varkud satellite.

10.1021/bi060337z CCC: $33.50
Published on Web 06/03/2006

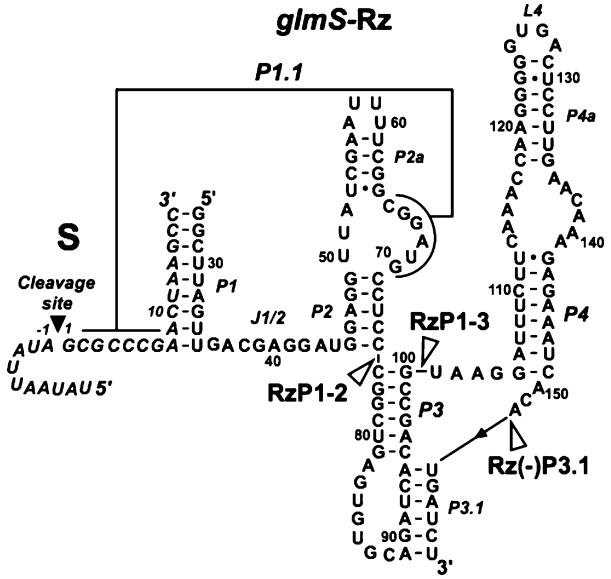

FIGURE 1: Predicted secondary structure of the *B. subtilis glmS* trans-cleaving construct based on sequence conservation within Gram-positive bacteria (*7*, *12*, *13*). Ribozyme and substrate strands are labeled *glmS*−Rz and S, respectively. The *B. subtilis glmS* mRNA contains a P1 terminal loop of 12 nucleotides. Nucleotide numbering of the ribozyme and substrate strands is taken from Breaker and co-workers (*1*). Nucleotides 5′ to the cleavage site are numbered starting with −1, consistent with the numbering of other self-cleaving catalytic RNAs such as the hairpin ribozyme and group I introns. The cleavage site is denoted with a black arrowhead. The sites and names for 3′-truncations of the ribozyme used in this study are denoted with white arrowheads.

ribozymes and the VS ribozyme (*7*, *15*). Transesterification is initiated through a nucleophilic attack of the 2′-hydroxyl of the nucleotide immediately 5′ to the cleavage site on the adjacent phosphodiester. A catalytically essential proton transfer role has been proposed for the amine functional group of GlcN6P (*11*). Otherwise, the chemical participants in this reaction are not known, but base functional groups have been clearly implicated in the reactions catalyzed by other ribozymes that use the same general catalytic strategy (*16*−*21*). Chemical probing of the *glmS* ribozyme has been limited to the use of in-line probing of the self-cleaving form in the presence and absence of the native ligand (*7*). The lone position on the RNA that responded to binding of the ligand was found in the joining region between P1 and P2, J1/2. It is not known if the reduction in the level of spontaneous cleavage at this site in Mg^{2+} is due to direct binding of GlcN6P or results from a conformational change that accompanies binding to a distal metabolite receptor. In the work presented here, we sought to define the level of conformational changes imparted to the riboswitch RNA upon ligand binding by use of hydroxyl radical probing and short-wave UV-induced cross-linking. These methods allow us to probe global tertiary structure at nucleotide resolution as well as local base−base stacking interactions within the catalytic motif under a variety of solution conditions.

MATERIALS AND METHODS

RNA Preparation. Substrate RNAs were generated on an Applied Biosystems DNA/RNA synthesizer using standard phosphoramidite chemistry from Glen Research. The RNA products were deprotected and then purified by denaturing PAGE and reverse phase HPLC as described previously (*22*). Ribozyme RNAs RzP1-2 and RzP1-3 were transcribed from partially double stranded templates as described previously (*23*). The *glmS*−Rz and Rz−P3.1 ribozymes were prepared by transcription of double-stranded DNA templates with T7 RNA polymerase. These templates were constructed by annealing two DNA strands each comprising half of the coding sequence that overlapped by 21 nucleotides from position 67 to 87, inclusive. A T7 RNA polymerase promoter was appended to the 5′-end of the 5′-primer to facilitate in vitro transcription. The 5′-overhangs were filled with Klenow DNA polymerase (Amersham) using the supplied buffer and then added to a PCR mixture containing appropriate primers. The PCR products were precipitated and the pellets resuspended in TE buffer [10 mM Tris-HCl (pH 8) and 0.1 mM EDTA (pH 8)]. The PCR product was then applied to a Sephadex G-50 column (equilibrated in TE buffer) for removal of salts and unincorporated deoxyribonucleotides and transcribed by T7 RNA polymerase as described previously (*24*). The volume for transcriptions of templates created in this manner was one-half the volume of the PCR.

Radiolabeled RNAs were prepared by phosphorylation of the 5′-terminal hydroxyl group with [γ-^{32}P]ATP (ICN) and polynucleotide kinase. Labeling of 3′-terminal hydroxyl groups was carried out with [α-^{32}P]cytidine 3′,5′-[5-^{32}P]-biphosphate (pCp) and RNA ligase as described previously (*25*). The pCp was made by phosphorylation of the 5′-hydroxyl group of 3′-CMP with [γ-^{32}P]ATP and polynucleotide kinase.

Hydroxyl Radical Footprinting Reactions. Ribozyme−substrate complexes were assembled in 50 mM sodium cacodylate (pH 7) at varying concentrations of $MgCl_2$ and GlcN6P (Sigma) in a final volume of 8 μL at room temperature and were allowed to equilibrate for 1 h. Increasing the time of incubation had no effect on the magnitude or identities of the hydroxyl radical protections. For these experiments, we employed 2×10^5 dpm (final concentration of <20 nM) of the labeled RNA and a final concentration of unlabeled RNA of 0.5 μM. The resulting complexes were treated with 0.7 μL of Fe(II)-EDTA [5 mM Na-EDTA (pH 8.0) and 5 mM $Fe(NH_4)_2(SO_4)_2$ prepared immediately prior to the experiment], 60 mM sodium ascorbate, and 0.38% (v/v) H_2O_2 as described previously (*26*). The reactions were quenched by adding 200 μL of a solution containing 0.3 M sodium acetate (pH 7), 0.1 μg/mL yeast tRNA (Sigma), and 600 μL of 100% ethanol. Following a 1 h precipitation at −70 °C, the quenched reaction products were recovered by microcentrifugation at 14 000 rpm for 20 min. Samples were resuspended in gel loading buffer, 95% (v/v) formamide, 25 mM EDTA, 0.01% (w/v) bromophenol blue, and 0.01% (w/v) xylene cyanol. The resuspended samples were then loaded onto sequencing gels.

Curve fitting of data sets from the normalized fraction protected versus the concentration of Mg^{2+} plots to the cooperative binding equation $f = f_{max} - [Mg^{2+}]^n/[[Mg^{2+}]^n + (K_d^{Mg})^n]$ was carried out exactly as described by Hampel and Burke (*27*).

Cross-Linking Analysis. UV cross-linking was carried out using a handheld 254 nm lamp (model UVG-54, UVP Inc.). Samples for analytical cross-linking were prepared in a final volume of 10 μL, containing 0.5 μM unlabeled substrate or ribozyme RNA, 1×10^6 dpm of 5′-end-labeled RNA (final

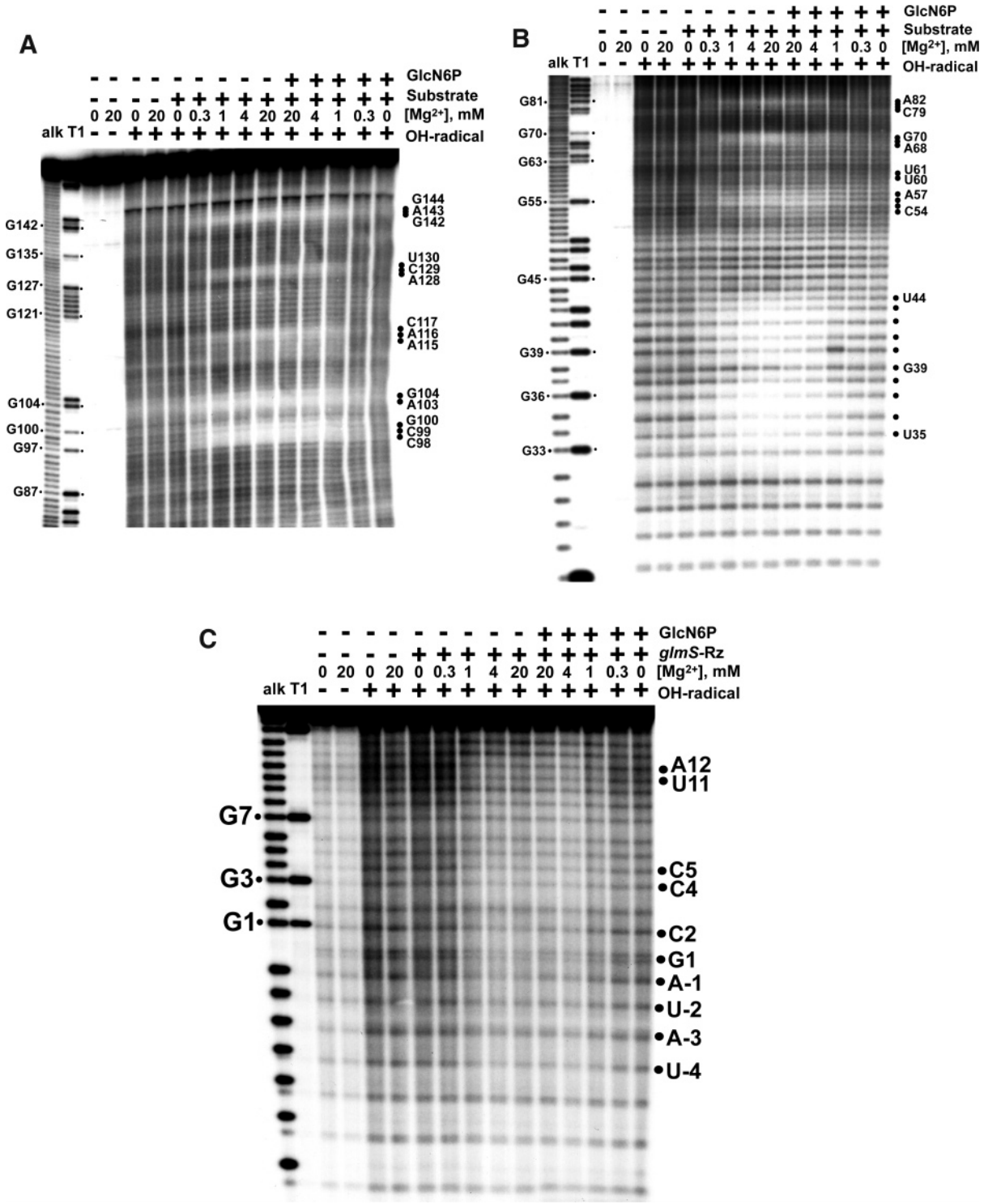

FIGURE 2: Hydroxyl radical protection of the *glmS* ribozyme−substrate complexes in Mg^{2+} is ligand-independent. Hydroxyl radical footprinting was performed on complexes formed with 5′-end-labeled *glmS*−Rz (A and B) and substrate (C) strands as described in Materials and Methods and then separated on 6 (A), 10 (B), and 20% (C) PAGE sequencing gels. Labeled ribozyme and substrate complexes, constituted as shown in the figure panels, were incubated in the presence or absence of varying concentrations of Mg^{2+} and 10 mM GlcN6P. The addition of GlcN6P did not affect the pattern of solvent protection or the magnitude of individual protections. The sites of protected residues were determined as described in Materials and Methods and are indicated at the right with black circles. The ribonuclease T1 and alkali hydrolysis sequencing ladders to the left of the panel are annotated by the location of several G residues. Since hydoxyl radical probing results in removal of the entire nucleotide at the site of attack, the identity of the protected nucleotide is shifted one band lower relative to the sequencing ladder. Thus, a protected site at G40 has a gel mobility identical to that of the G39 ribonuclease T1 digestion product.

concentration of ~40 nM), 25 mM Mg^{2+}, and 50 mM Tris-HCl (pH 7.5), and incubated at 25 °C for 1 h. The samples were then pipetted into 96-well microtiter plate wells and irradiated 1 cm from the UV source at room temperature for 3 min. To prepare isolated cross-linked RNAs, the reaction described above was scaled up to a volume of 100 μL without any change in the concentrations of the components except that ~1 × 10^8 dpm of 5′- or 3′-end-labeled RNA was employed (final concentration of 0.5 μM). These samples were aliquoted into 10 wells of a 96-well microtiter

plate and irradiated as described above for 8 min. The aliquots were pooled and applied to a Centrisep (Princeton Separations) gel exclusion column equilibrated in distilled deionized H_2O (ddH_2O) and microcentrifuged for 3 min at 3000 rpm. An equal volume of formamide gel loading buffer was added to the eluted samples, and the cross-linked RNAs were separated on 8% denaturing gels. Individual cross-links were visualized by autoradiography and recovered from the gels as described previously (*28*). Mapping the sites of cross-linking was performed as described previously (*28*).

The kinetics of self-cleavage were determined by mixing purified cross-linked RNAs resuspended in ddH_2O with an equal volume of reaction buffer so that the final concentrations were 25 mM Mg^{2+} and 25 mM Tris-HCl (pH 7.5) with or without 10 mM GlcN6P in a final volume of 15 μL. Reactions were allowed to proceed at 25 °C, and 1 μL aliquots were quenched at the indicated time points into gel loading buffer on ice. The self-cleavage rate (k_{obs}) was calculated by fitting the plots of fraction cleaved versus time as described previously to single- or double-exponential equations (*29*).

RESULTS

Our initial aim was to probe the *glmS* ribozyme RNA tertiary structure in the presence and absence of ligand by hydroxyl radical footprinting. Hydroxyl radicals attack C4′ of ribose and initiate a chemical reaction that results in strand scission (*30*−*32*). Since this site is accessible in double-stranded RNA, the reagent can be used to study nucleotide-level solvent accessibility for the entire RNA of interest (*33*). Radiolabeled RNA products of hydroxyl radical probing can be separated on PAGE sequencing gels, quantified, and compared to those from unfolded RNA to examine the solvent accessibilities of sites in a structured RNA at single-nucleotide resolution. Since binding of small molecule ligands in other riboswitch systems results in significant changes in the secondary and tertiary structure of the RNA receptor, we reasoned that hydroxyl radical probing could be employed to map the changes in structure induced by binding of GlcN6P to the *Bacillus subtilis glmS* ribozyme. These folding experiments cannot be conducted on cleavable ribozyme−substrate complexes since the cleavage of the scissile linkage, particularly in the presence of ligand where the reaction is greatly accelerated, would obscure the footprinting data obtained with a labeled RNA that carries the cleavage site. Likewise, if labeled ribozyme were to be footprinted in the presence of a cleavable substrate and ligand, cleavage of the substrate would possibly allow the highly conserved residues 5′ to the cleavage site to dissociate from the complex (*7*). We therefore chose to conduct our experiments on a trans-acting ribozyme−substrate complex with a chemically synthesized substrate containing a 2′-deoxy substitution of the nucleotide immediately 5′ to the cleavage site, A-1. This substitution renders the scissile bond non-cleavable by internal nucleophile attack. Photo-cross-linking of these constructs shows that identical sites are cross-linked with cleavable, all-ribose substrates and with the substrates containing the 2′-deoxy A-1 substitution (data not shown). This suggests that this 2′-deoxy substitution does not interfere with the formation of the native ribozyme−substrate structure formed in Mg^{2+}. Although the *glmS* mRNA motif contains conserved bases as many as 60 nucleotides upstream of the cleavage site, to keep the substrate sufficiently short to be synthesized chemically, we chose the substrate previously used by Breaker and co-workers which terminates at position −10 relative to the cleavage site (*2*, *7*). The ribozyme strand was truncated nine nucleotides beyond the end of P4. This enabled us to retain the conserved pseudoknot structure, P3.1 (*13*, *14*).

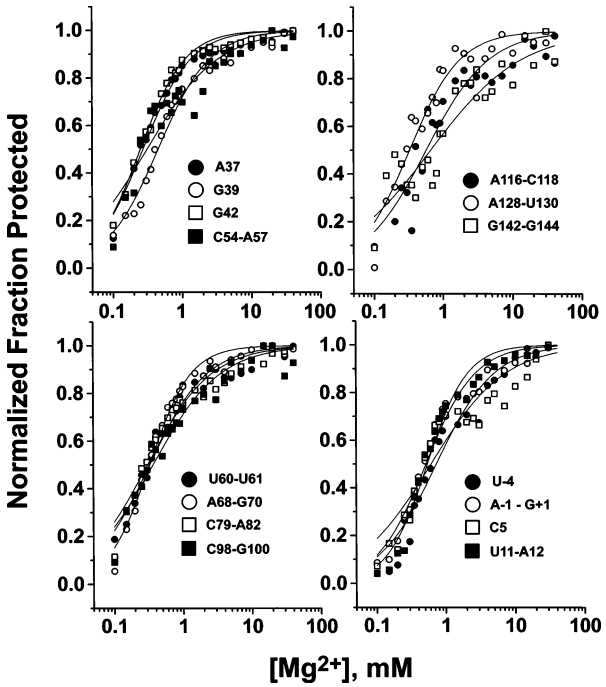

FIGURE 3: Mg^{2+} titrations of hydroxyl radical footprinting reveal that all sites of solvent protection are half-saturated at <1 mM Mg^{2+}. The fractional hydroxyl radical protection at each site on the backbone of the ribozyme and substrate was calculated as described previously (*27*). These data were then normalized so that the highest level of protection at each site was given a value of 1 and plotted as a function of the Mg^{2+} concentration. Each data point represents an average of at least two independent measurements. The actual magnitudes of protection ranged between 0.35 and 0.80. Each data set was fit to the cooperative binding equation $f = f_{max} - \{[Mg^{2+}]^n/([Mg^{2+}]^n + (K_d^{Mg})^n]\}$. The resulting curve fits can be used to extrapolate the range of the Mg^{2+} dependence for protection at each well-protected site in the ribozyme−substrate complex. The results from three to four different sites of backbone protection are plotted in each panel.

The hydroxyl radical probing experiments were conducted by incubating the labeled ribozyme strand or substrate strand with its pairing partner in the presence or absence of Mg^{2+} with or without added GlcN6P. We used a GlcN6P concentration that was shown to be saturating for the ribozyme cleavage reaction (data not shown) under similar ionic conditions and with identical constructs. Figure 2 shows the results of representative footprinting experiments. Upon addition of Mg^{2+}, several areas on the ribozyme−substrate complex are protected from hydroxyl radical-mediated strand scission. Folding in the presence or absence of GlcN6P as a function of Mg^{2+} concentration did not reveal any specific, reproducible differences in the degree of solvent protection at specific sites or the identities of the protected sites. We can envision two testable hypotheses that could be evidenced by this result.

First, the footprinted structure reports on a dominant non-native structure that does not bind ligand. Evidence that a single, dominant structure is observed is twofold. First, the

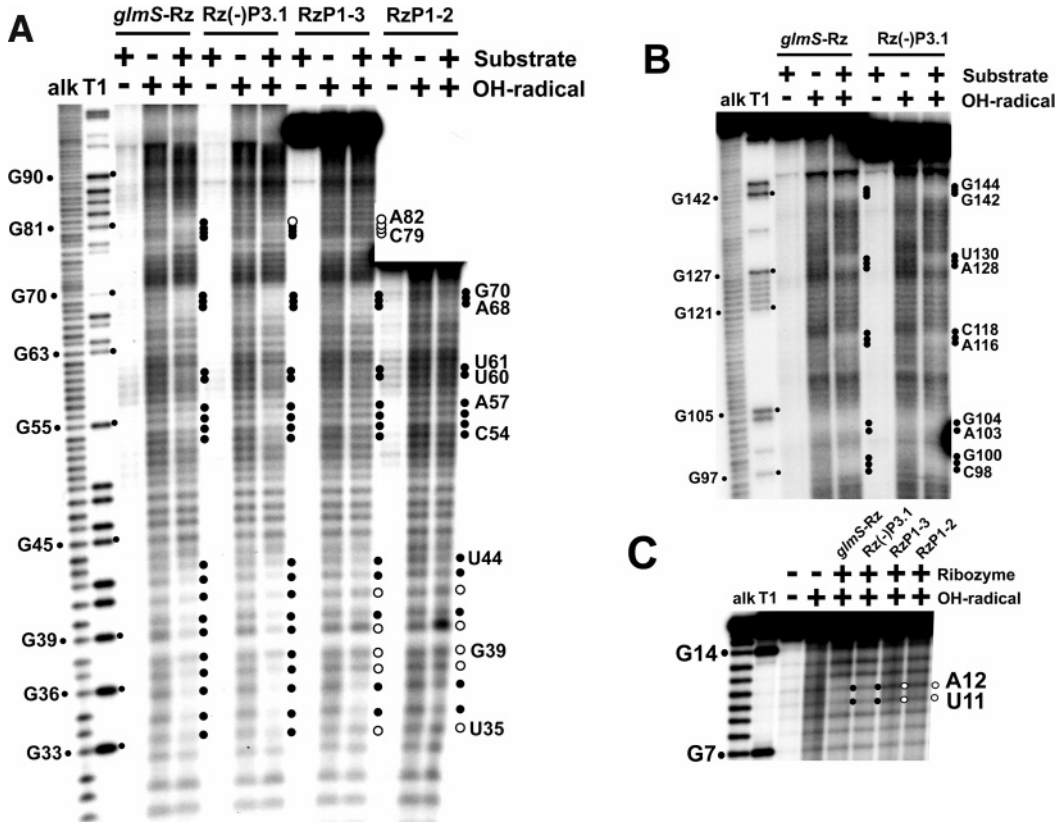

FIGURE 4: Hydroxyl radical protection of ribozyme−substrate complexes formed with 3′-truncated ribozymes defines points of additional RNA packing with longer constructs. End-labeled ribozyme (panels A and B) and substrate (C) were folded in the presence of 25 mM Mg^{2+} and then subjected to hydroxyl radical probing as described in Materials and Methods. The products of these reactions were separated on 10 (A), 6 (B), and 20% (C) sequencing gels. Negative control complexes for ribozyme and substrate folding were assembled in Mg^{2+} in the absence of unlabeled substrate and ribozyme, respectively. The sites of protection in the various complexes are indicated at the right of each set of ribozyme-specific data with a small black circle. White circles indicate the sites that are not protected in the individual truncated complex but that are protected in the *glmS*−Rz construct-containing complexes. Base references for protected sites are listed at the right of each panel.

magnitude of solvent protection at individual sites is very strong, between 35 and 80%, at saturating concentrations of Mg^{2+} (data not shown). Second, Mg^{2+} titrations reveal that all sites become half-saturated at concentrations of Mg^{2+} that vary by less than 5-fold (0.2−1 mM) (Figure 3). These observations are difficult to reconcile with the suggestion that the solvent protections arise from an ensemble of native and non-native structures. If multiple alternative tertiary forms of the complex were present in solution, we would expect to find that the magnitude of protection at specific sites would be lower than that which we observe and that the protected regions would become saturated over a wider range of Mg^{2+} concentrations, reflecting a variation in the stabilities of more than one unrelated structure.

If a single solution structure is defined by these probing experiments, how can we be certain that the data report on the native structure of the catalytic motif? First, we find that many of the sites of protection correspond to the highly conserved regions of the ribozyme and substrate strands as expected if these conserved elements interact with one another to form the active fold. These sites include the entire highly conserved 5′-GACGAGG-3′ sequence in J1/2 which is very well protected from solvent in our experiments (*7*). Second, the observation that binding of the substrate is required for solvent protection of ribozyme and vice versa suggests that we are observing the native form of the complex since essential catalytic elements are required. Another way to examine this question would be to study to structure of truncated ribozyme constructs. The minimal catalytic form of the *glmS* ribozyme extends from the cleavage site to the end of P2 (*7*). If the solvent protections that we have observed in our *glmS*−Rz construct are indeed the result of native tertiary interactions, a significant subset of them should be found upon probing of this minimal variant and other 3′-truncated ribozymes. The results in Figure 4 demonstrate that many of the protected sites in the *glmS*−Rz construct are also found when the RzP1-2 and RzP1-3 ribozyme-substrate constructs are probed. These results are summarized in Figure 5. In addition, while the *glmS*−Rz ribozyme has more solvent-protected regions than the 3′-truncated ribozymes, likely due to folding of the P3 and P4 structures upon the minimal catalytic structure, we find no protected sites that are unique to the minimal form. This observation further argues that our data for the minimal ribozyme define a native tertiary structure. These results also indicate possible points of direct interaction between the nonessential 3′-conserved domain comprising P3 and P4, termed domain 2 (*7*), and the core of the ribozyme. This includes conserved base pairs in P1 and specific regions of the highly conserved J1/2 segment which are protected in the longer constructs. We also note that the Mg^{2+} dependence for folding of the minimal RzP1-2 constructs is much greater than of longer constructs and that the minimal ribozyme is generally more solvent accessible even at concentrations of Mg^{2+} that

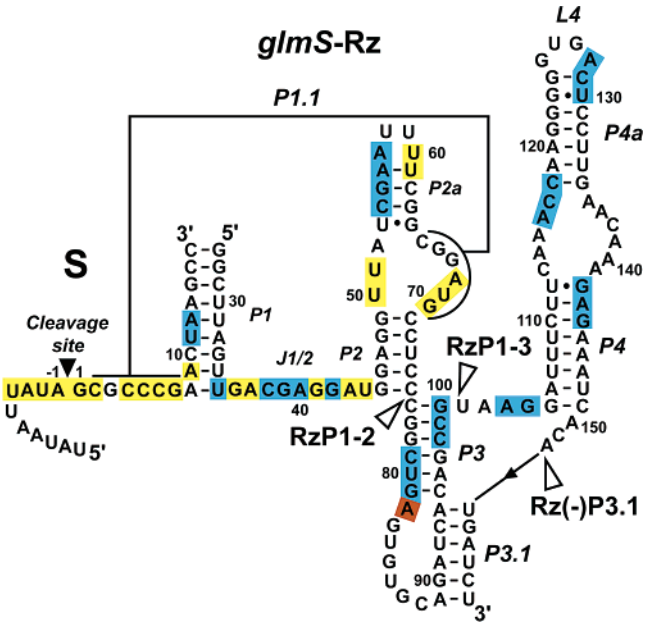

FIGURE 5: Summary of the hydroxyl radical footprinting results. Shaded areas are protected from hydroxyl radical attack in ribozyme−substrate complexes. Nucleotides highlighted in yellow are protected in all constructs studied in this work; nucleotides highlighted in blue are protected in only the *glmS*−Rz and Rz−P3.1 constructs, and the nucleotide highlighted in orange is protected in the *glmS*−Rz construct alone.

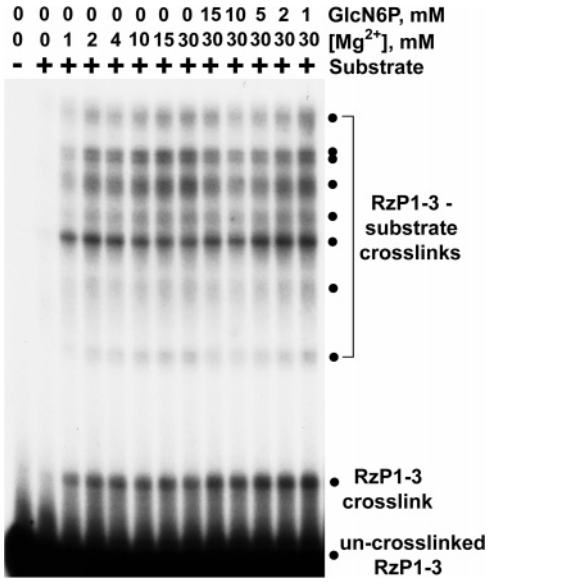

FIGURE 6: Cross-linking pattern of *glmS* ribozyme−substrate complexes that is unaffected by the presence of GlcN6P. [^{32}P]Rz−P1-3 complexes were prepared at various concentrations of Mg^{2+}, GlcN6P, and 2′-deoxy A-1-modified substrate as described in Materials and Methods and allowed to equilibrate for 1 h at room temperature prior to being irradiated with UV (254 nm) light. The products were separated on an 8% denaturing PAGE gel. The positions of cross-linked products and the un-cross-linked ribozyme are indicated at the right. Most of the cross-linked products link the Rz−P1-3 construct to the substrate, and one major cross-link forms between two separate sites on the ribozyme strand.

approach saturation (Figure 4, data not shown). Likewise, the Mg^{2+} dependence of the cleavage reaction rate for the *glmS*−Rz construct is markedly lower than that of the RzP1−2 construct (*13*, *14*; M. M. Tinsley and K. J. Hampel, unpublished observations).

The second hypothesis that we can put forward to explain the lack of solvent protection unique to a ligand-bound complex is that the magnitude of the conformational change induced by ligand binding is nonexistent or cannot be detected by the method. Since we were not able to observe differences between the unbound and ligand-bound forms of the ribozyme−substrate complex by footprinting, we turned to photo-cross-linking with short-wave UV light to define points of contact between the RNA components and possibly differences between the apo and ligand-bound forms of the ribozyme−substrate complex. UV cross-linking has been used in many ribozyme systems to define points of direct interaction or closely juxtaposed bases in three-dimensional space (*28*, *34*−*37*). In the hammerhead ribozyme system, it has been possible to cross-link bases that are involved in structures that are predicted to be very short-lived or not favored at equilibrium (*38*). Thus, it may be possible in the *glmS* system to define specific points of difference between the ligand-bound and unbound ribozymes that cannot ne detected by methods, such as equilibrium footprinting, which monitor the formation of stable structures. In addition, we wanted to identify covalently cross-linked sites and determined if these trapped structures retain catalytic activity. Those that retain catalytic activity identify constraints in structure that are compatible with the active ribozyme tertiary structure.

While some cross-linking strategies employ tethered cross-linking agents capable of acting at distances of several angstroms (*28*, *39*), we chose to apply short-wavelength UV light (254 nm) to trap direct contacts between stacked nucleobases (*40*). In this way, we could negate, as much as is possible, the ability of the RNA to compensate for non-native interactions through its inherent flexibility, as described for the *Tetrahymena* group I intron (*41*). In our initial screens for UV-induced cross-links, ^{32}P-labeled ribozyme−substrate complexes formed in the presence or absence of GlcN6P and Mg^{2+} were exposed to 254 nm UV light for short periods of time (3 min) and analyzed on denaturing gels. Several cross-links were formed under these conditions, most of which required the presence of Mg^{2+}, but we did not observe cross-links that were dependent upon or were inhibited by the presence of GlcN6P (Figure 6). This preliminary data generally confirmed our results obtained through footprinting analysis, but since the data were negative, we were again left with the concern that nondetectable conformational changes could be taking place as a result of ligand binding. In addition, since it is possible that more than one cross-link can comigrate on these gels, information about ligand-specific cross-links can be lost.

To test the emerging idea that the ribozyme−substrate complex can fold into a native structure that can subsequently bind ligand productively without inducing significant conformational changes, we required a positive assay. Since we observed no gross differences between complexes cross-linked in the presence or absence of ligand, we reasoned that it might be possible to cross-link cleavable ribozyme−substrate complexes in the absence of ligand and then catalytically activate them upon incubation with the ligand. This would provide evidence for the formation of a stable ligand binding pocket that can form in the absence of GlcN6P. Figure 7A shows the results of one of these experiments. Results using the RzP1-3 ribozyme construct are shown here since it was with this construct that we were

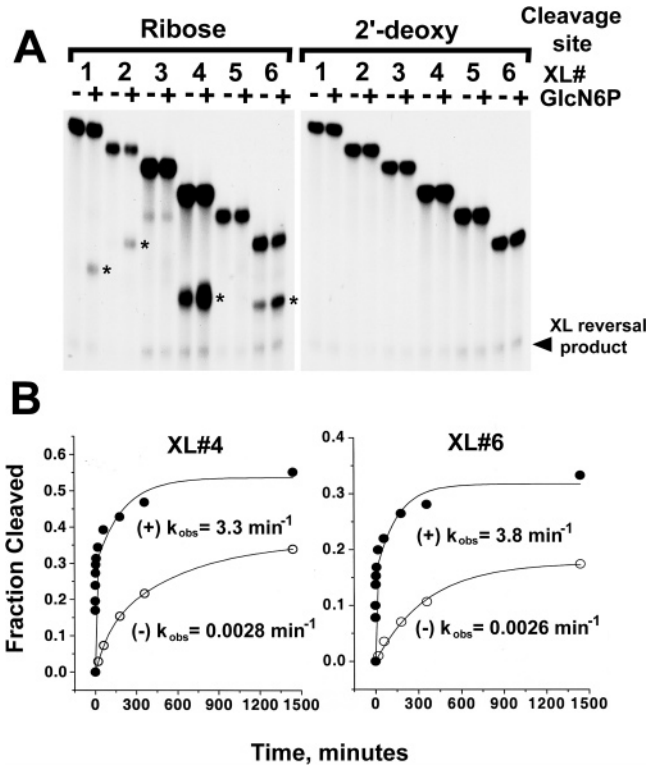

FIGURE 7: Isolated cross-linked ribozyme−substrate complexes can be stimulated to self-cleave in the presence of GlcN6P. (A) Complexes consisting of 5′-end-labeled ribozyme cross-linked to unlabeled substrate (XL 1−6) were incubated overnight in cleavage buffer [50 mM Tris-HCl (pH 8) and 20 mM Mg^{2+}] in the presence or absence of 10 mM GlcN6P and then separated on denaturing 8% PAGE gels. Specific cleavage products that predominate in ligand-containing reaction mixtures are denoted with asterisks and are not observed when the cleavage site is 2′-deoxy-modified (compare left and right panels). Each cross-linked product reversed to a limited degree during cross-link isolation so that the 5′-end-labeled ribozyme, or reversal product, can be seen at the bottom of each panel. (B) Kinetics of self-cleavage of XL 4 and XL 6 with or without GlcN6P. Isolated cross-links were incubated in buffer containing 50 mM Tris-HCl (pH 7.5) and 25 mM $MgCl_2$ for the indicated times in the presence (+) or absence (−) of 10 mM GlcN6P at 25 °C. The fraction of self-cleaved cross-linked complexes was determined and plotted as a function of time, and the data were curve fit as described in Materials and Methods.

able to achieve the best electrophoretic separation of the cross-linked products. By labeling only the ribozyme RNA, we are restricted to monitoring the cleavage of the substrate under conditions where the cross-link between the two RNAs is preserved during the cleavage reaction.

Ribozyme−substrate complexes in which the ribozyme is labeled were allowed to fold in Mg^{2+}-containing buffers for 1 h and then exposed to UV light for several minutes (see Materials and Methods). The products were separated on preparative denaturing PAGE gels, excised from the gels, eluted, and precipitated. The purified cross-linked ribozyme−substrate complexes were then resuspended in Tris buffer and treated with Mg^{2+} in the presence or absence of GlcN6P. We were able to carefully control for the site specificity of ligand-dependent cleavage by conducting parallel experiments in which the native scissile linkage was protected from cleavage by 2′-deoxy modification (Figure 7A, right panel). Complexes formed from noncleavable substrates do not show any cleavage products, but four of the complexes formed with all ribose substrates were cleaved preferentially upon incubation with GlcN6P. The levels of cleavage in the presence and absence of GlcN6P lead us to believe that the catalytic motif retained some level of ligand dependence even when constrained by cross-linking specific bases. We were intrigued, however, by the high apparent level of catalysis by two cross-linked species in the absence of ligand (cross-links 4 and 6). Catalysis in the absence of ligand could imply that we had trapped a ligand-independent form of the complex. To inspect the catalytic activities of these species further, we carried out kinetic analysis of self-cleavage in the presence and absence of GlcN6P (Figure 7B). The results confirmed that these cross-linked species were significantly dependent on GlcN6P for activity. Incubation with ligand increased the cleavage rate of XL 4 and XL 6 by >1000-fold relative to the rate achieved in Tris buffer and Mg^{2+} alone (*7*, *11*). It should be noted that Tris has been shown to stimulate *glmS* self-cleavage, most likely by acting as a ligand coenzyme in the reaction (*11*). Thus, our observation of observable site-specific *glmS* cleavage in Tris buffer is not surprising. The cleavage rates reported in Figure 6 for XL 4 and XL 6 at pH 8 could not be directly compared to the rate of the un-cross-linked ribozyme since its rate is to fast to be measured by hand mixing. However, given the published rate−pH profile of the *glmS* ribozyme, we can extrapolate from the cleavage rate of 1 min^{-1} that we observe for the un-cross-linked ribozyme at pH 5.5 at identical Mg^{2+} and GlcN6P concentrations (data not shown). Correcting for the increase in rate from pH 5.5 to 7.5, we arrive at a predicted cleavage rate of ∼100 min^{-1} at pH 7.5. This value is ∼30-fold faster than the rates observed for the cross-linked products. The low amplitude of cleavage for the cross-linked ribozymes, 30−50%, is consistent with the effect of RNA lesions induced by prolonged exposure to short-wave UV light. We have observed a similar loss of cleavage amplitude in hairpin ribozyme complexes exposed to 254 nm light (*36*).

The identities of the cross-linked bases were mapped by subjecting the labeled cross-linked species to limited alkaline hydrolysis and then separating the products on a sequencing gel. These hydrolysis ladders terminate at the nucleotide involved in the cross-linking event (*28*). Two of the active cross-linked forms and two inactive cross-links could be mapped in this manner. Cross-link 2 maps from U59 of the ribozyme strand to U11 in the P1 helix portion of the substrate, defining a close approach of these bases or a native tertiary structure between the L2 loop and P1 (Figure 8). The second active cross-link, XL 4, mapped to G1, the base immediately 3′ to the cleavage site, and U44. Mapping of the cross-link to G1 is complicated somewhat by the presence of an additional cutoff at G3. Mapping of the cross-link using 3′-end-labeled substrates, however, did not show any strong cutoff at G3 but confirmed the involvement of G1 in this cross-link (data not shown). Thus, it seems that the G3 cross-link is a minor cross-linked form. The observation of a cross-link from the active site of the ribozyme to a distant element of the complex helps us to define elements of the ribozyme active site distal to the nucleotides adjacent to the cleavage site. Catalytically inactive cross-links also mapped to the invariant cleavage site guanosine, G1. The ribozyme sites of these cross-links mapped to G36 and G55. Unfortunately, XL 6 could not be mapped since the mobility of the cross-link reverted to that of the un-cross-linked RNA after partial alkaline hydrolysis. XL 1, though active, could not be

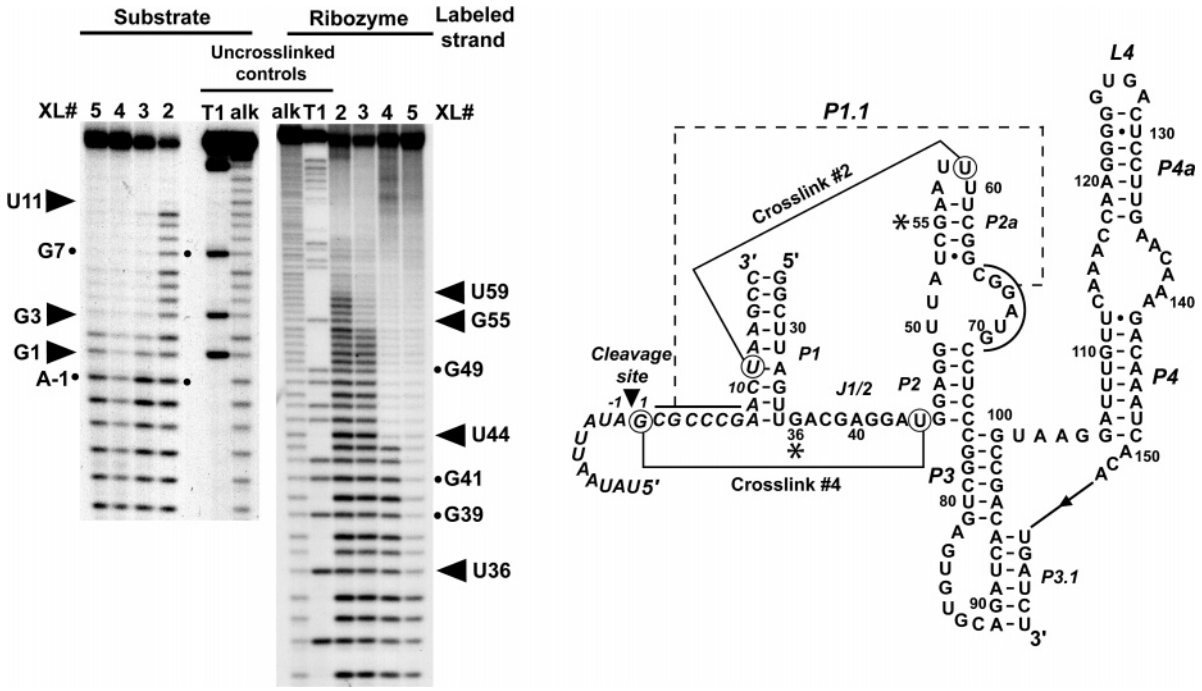

FIGURE 8: Nucleotide mapping of cross-links 2−5 on the substrate and ribozyme strands. (A) Purified cross-linked RNAs (XL 2−XL 5) derived from 5′-end-labeled substrate (left) and ribozyme (right) were subjected to alkali hydrolysis, and the products were separated on denaturing PAGE gels. Non-cross-linked control RNAs were treated with alkali and ribonuclease T1 and were run in parallel (innermost lanes in both panels). Sites of cross-linking are denoted with black arrowheads to the side of each panel and are annotated by the base designation. (B) Secondary structure of the *B. subtillis glmS* ribozyme with the sites of cross-linking indicated. Lines connect bases that can be cross-linked to form a catalytically active complex between the ribozyme and substrate. Asterisks denote bases (G36 and G55) that can be cross-linked to G1, forming inactive complexes.

mapped efficiently as well. It should be noted that we identified all of the major cross-linked species in the minimal ribozyme (RzP1-2) and the *glmS*−Rz construct in addition to the RzP1-3 construct. Thus, the cross-links appear to represent common folded structures or kinetic folding intermediates.

DISCUSSION

The *glmS* ribozyme is among a class of mRNA elements, the riboswitches, that effect a change in gene expression in response to ligand binding (*1*, *3*). Prior to the discovery of the *glmS* ribozyme, all known naturally occurring riboswitches had been shown to function by ligand-induced conformational change. Current evidence for these allosteric effector riboswitches supports a model in which the unbound mRNAs exist predominantly in a structure that is different from the ligand-bound form, and the structural differences between the bound and unbound forms dictate the effect on gene expression (*1*). An important question of the *glmS* system is, therefore, whether this riboswitch functions similarly. Put another way, the question is whether GlcN6P acts as an allosteric effector or a coenzyme. Recent data from the Soukup laboratories point to the direct involvement of the ligand in the cleavage reaction (*11*). Such coenzyme involvement in catalysis does not necessarily require large-scale conformational rearrangement of the active site. Here we present complementary data showing that the riboswitch can fold into the active tertiary structure in a manner independent of the GlcN6P binding. Our evidence support the hypothesis that the ligand binds to a prefolded active site. In addition, we have implemented the use of structure probing methods, hydroxyl radical footprinting and photo-cross-linking, to monitor tertiary folding of the *glmS* ribozyme. We expect that these tools will be very useful in defining the roles of catalytically important nucleotides within the *glmS* ribozyme and following the RNA folding pathway, as shown in other ribozyme systems (*16*, *29*, *42*, *43*).

A combination of structural measurements was used to determine the magnitude of the conformational change within the riboswitch RNA as a function of added ligand. We found no clear evidence of a conformational change expected if the ligand acts as an allosteric effector. Though the successful implementation of hydroxyl radical probing to this system provides a useful tool for assaying the native structure of the ribozyme, our results constitute negative data with respect to the question of a ligand-induced conformational change within the active complex. Indeed, in addition to the two hypotheses presented above to explain this lack of ligand-dependent probing results, the third possibility is that ligand is not stoichiometrically bound by the complex under the conditions used in these assays. This could be the case if, for example, the concentration of ligand required to saturate a ribozyme cleavage assay with an all-ribose substrate is not sufficient to saturate a complex containing a 2′-deoxy-modified cleavage site. Evidence for a direct role of the ligand in the chemistry of the cleavage reaction makes it more likely that GlcN6P binds at or very near the active site; thus, changes to the sugar pucker and the loss of a hydrogen bond delivered by the 2′-deoxy substitution cannot be overlooked. Further work will be required to develop assays for binding of ligand to these catalytically inert mutants so that we can isolate the individual steps in the reaction pathway, such as ligand binding, from the chemical cleavage step.

Nevertheless, we were able to overcome the systematic limitations of the probing data to address our central question regarding the RNA conformation in the presence and absence of ligand. Since the appearance of the covalent cross-links that we observed was ligand-independent, and we could assay covalently cross-linked RNAs for catalytic activity in a very well controlled manner, we chose to characterize the ability of cross-linked RNAs to be activated to self-cleave by addition of ligand. We identified two distinct covalent cross-links within the minimal ribozyme motif that were capable of catalytic activation by GlcN6P. Thus, a model can be put forward in which, upon incubation with appropriate folding cations, the riboswitch presents a preformed ligand binding pocket to which the ligand binds without inducing large-scale changes in RNA tertiary structure. The in vitro selected Diels−Alder ribozyme similarly presents a preformed binding pocket for its substrate upon incubation in a folding solution (*44*, *45*). In contrast, previously characterized bacterial riboswitches and several in vitro-derived aptamers are not predominantly prefolded into a ligand binding conformation in the absence of the ligand (*1*, *5*, *46*, *47*). In these aptamer−ligand complexes, ligand binding induces the formation of a complex tertiary structure or captures a specific tertiary structure. The recently reported structures of the three purine riboswitches make it seem very unlikely that a prefolded ligand binding pocket could admit these bases since the ligands are surrounded on all sides by RNA (*48*, *49*).

We have identified two covalent cross-links that fix the ribozyme−substrate complex into a form that can productively bind GlcN6P. The identities of these cross-links tell us about the native tertiary structure of the *glmS* ribozyme. One of these is an active site cross-link that covalently fixes the base immediately 3′ to the cleavage site, G1, to the nonconserved U44 located at the 3′-end of J1/2. The A43−U44 phosphodiester linkage was previously shown to be susceptible to a spontaneous in-line cleavage event that is quenched by the presence of the ligand (*7*). If GlcN6P binds at or near the active site, as expected of a coenzyme, then our cross-linking data which link the cleavage site and J1/2, combined with the in-line probing results, suggest that J1/2 is a ligand binding element. It is noteworthy that J1/2 is the longest and most highly conserved single-stranded segment in the minimal ribozyme motif. Though binding of the ligand could be specified in part by specific, conserved double-stranded regions of the RNA, it is more likely that an essential, highly conserved single-stranded region comprises the bulk of a ligand binding pocket, as observed with other small molecule binding RNAs (*48*, *50*−*52*). The cleavage rate of this cross-linked form is within 30-fold of the estimated rate of the un-cross-linked ribozyme under identical conditions. In the hairpin ribozyme system, an active site cross-link, G8−A-1, which correlates strongly with base stacking seen in high-resolution structures, has been shown to achieve a cleavage rate constant ~100 fold lower than the wild-type rate (J. E. Heckman and J. M. Burke, personal communication) (*53*). Thus, the rate constant of XL 4 is within the range that we expect of a native base stacking interaction. Two prominent inactive cross-links that link G1 to sites in the ribozyme, G36 and G55, were identified. It is difficult to reconcile these cross-links with the active cross-link between G1 and U44, particularly if one considers the proposed pseudoknot interaction between the nucleotides immediately 3′ to G1 and J2a/2 that has been proposed (*11*). It is possible that these two inactive cross-links represent structures at an early step in the native folding pathway for the ribozyme, but such a hypothesis would be very difficult to test experimentally.

In contrast to the active site cross-link described above, the catalytically active U11−U59 pair traps helical elements peripheral to the active site. U11 is located within P1 and is part of a phylogenetically conserved set of base pairs, 5′-$C_{10}U_{11}$-3′ and 5′-$A_{32}G_{33}$-3′. We initially speculated that the conserved GUGA tetraloop that caps P4 would interact with this double-stranded receptor in P1. GUGA tetraloops preferentially interact with this double-helical sequence (*54*, *55*). This hypothesis is bolstered by the finding that the hydroxyl radical protection of a P1 sequence that overlaps this conserved dinucleotide motif is observed only in ribozyme constructs that contain the P4 domain (Figure 4). Our cross-linking data, however, also point to at least a transient interaction between L2 and P1 that is consistent with the active tertiary structure of the ribozyme. In addition to the P1 solvent protection, we have observed several points of solvent protection that are due to the folding of the P4 stem−loop structure. These certainly represent at least some direct interactions between P4 and the minimal catalytic sequence as well as additional compaction of the minimal motif that results from folding of all the conserved structural elements. However, we have noted no change in the affinity of the ligand for the ribozyme in the minimal ribozyme relative to the *glmS*−Rz construct (M. M. Tinsley and K. J. Hampel, unpublished observations); thus, we cannot speculate that any of the P4-dependent protections in J1/2 are involved in ligand recognition.

The evolutionary origin of the *glmS* riboswitch is an important question. Our data support the hypothesis that the *glmS* ribozyme forms a prefolded RNA pocket to which GlcN6P binds without inducing large-scale conformational changes. The implication of this idea is that the *glmS* riboswitch may have evolved a stable ligand binding domain and catalytic activity properties simultaneously. The alternative hypothesis would be that an evolutionary predecessor for the current *glmS* riboswitch used GlcN6P binding to effect a conformational change as observed in most naturally occurring riboswitches (*1*). Additional changes optimized the ligand binding pocket such that GlcN6P could function more directly in catalysis, as seen currently (*11*).

ACKNOWLEDGMENT

We thank Dr. John M. Burke for generously supporting this independent line of research, Joyce Heckman for providing helpful discussions, and Anne MacLeod for assistance in the preparation of the manuscript.

REFERENCES

1. Winkler, W. C., and Breaker, R. R. (2005) Regulation of bacterial gene expression by riboswitches, *Annu. Rev. Microbiol. 59*, 487−517.
2. Barrick, J. E., Corbino, K. A., Winkler, W. C., Nahvi, A., Mandal, M., Collins, J., Lee, M., Roth, A., Sudarsan, N., Jona, I., Wickiser, J. K., and Breaker, R. R. (2004) New RNA motifs suggest an expanded scope for riboswitches in bacterial genetic control, *Proc. Natl. Acad. Sci. U.S.A. 101*, 6421−6426.

3. Nudler, E., and Mironov, A. S. (2004) The riboswitch control of bacterial metabolism, *Trends Biochem. Sci. 29*, 11−17.
4. Sudarsan, N., Barrick, J. E., and Breaker, R. R. (2003) Metabolite-binding RNA domains are present in the genes of eukaryotes, *RNA 9*, 644−647.
5. Winkler, W., Nahvi, A., and Breaker, R. R. (2002) Thiamine derivatives bind messenger RNAs directly to regulate bacterial gene expression, *Nature 419*, 952−956.
6. Mironov, A. S., Gusarov, I., Rafikov, R., Lopez, L. E., Shatalin, K., Kreneva, R. A., Perumov, D. A., and Nudler, E. (2002) Sensing small molecules by nascent RNA: A mechanism to control transcription in bacteria, *Cell 111*, 747−756.
7. Winkler, W. C., Nahvi, A., Roth, A., Collins, J. A., and Breaker, R. R. (2004) Control of gene expression by a natural metabolite-responsive ribozyme, *Nature 428*, 281−286.
8. Doudna, J. A., and Cech, T. R. (2002) The chemical repertoire of natural ribozymes, *Nature 418*, 222−228.
9. Cech, T. R. (1990) Self-splicing of group I introns, *Annu. Rev. Biochem. 59*, 543−568.
10. Celander, D. W., and Cech, T. R. (1991) Visualizing the higher order folding of a catalytic RNA molecule, *Science 251*, 401−407.
11. McCarthy, T. J., Plog, M. A., Floy, S. A., Jansen, J. A., Soukup, J. K., and Soukup, G. A. (2005) Ligand requirements for glmS ribozyme self-cleavage, *Chem. Biol. 12*, 1221−1226.
12. Soukup, G. A. (2006) Core requirements for glmS ribozyme self-cleavage reveal a putative pseudoknot structure, *Nucleic Acids Res. 34*, 968−975.
13. Wilkinson, S. R., and Been, M. D. (2005) A pseudoknot in the 3′ non-core region of the glmS ribozyme enhances self-cleavage activity, *RNA 11*, 1788−1794.
14. Roth, A., Nahvi, A., Lee, M., Jona, I., and Breaker, R. R. (2006) Characteristics of the glmS ribozyme suggest only structural roles for divalent metal ions, *RNA 12*, 607−619.
15. Fedor, M. J., and Williamson, J. R. (2005) The catalytic diversity of RNAs, *Nat. Rev. Mol. Cell Biol. 6*, 399−412.
16. Pinard, R., Hampel, K. J., Heckman, J. E., Lambert, D., Chan, P. A., Major, F., and Burke, J. M. (2001) Functional involvement of G8 in the hairpin ribozyme cleavage mechanism, *EMBO J. 20*, 6434−6442.
17. Nakano, S., Chadalavada, D. M., and Bevilacqua, P. C. (2000) General acid−base catalysis in the mechanism of a hepatitis delta virus ribozyme, *Science 287*, 1493−1497.
18. Pinard, R., Lambert, D., Heckman, J. E., Esteban, J. A., Gundlach, C. W., IV, Hampel, K. J., Glick, G. D., Walter, N. G., Major, F., and Burke, J. M. (2001) The hairpin ribozyme substrate binding-domain: A highly constrained D-shaped conformation, *J. Mol. Biol. 307*, 51−65.
19. Das, S. R., and Piccirilli, J. A. (2005) General acid catalysis by the hepatitis delta virus ribozyme, *Nat. Chem. Biol. 1*, 45−52.
20. Perrotta, A. T., Shih, I., and Been, M. D. (1999) Imidazole rescue of a cytosine mutation in a self-cleaving ribozyme, *Science 286*, 123−126.
21. Shih, I. H., and Been, M. D. (2001) Involvement of a cytosine side chain in proton transfer in the rate-determining step of ribozyme self-cleavage, *Proc. Natl. Acad. Sci. U.S.A. 98*, 1489−1494.
22. Walter, N. G., Yang, N., and Burke, J. M. (2000) Probing non-selective cation binding in the hairpin ribozyme with Tb(III), *J. Mol. Biol. 298*, 539−555.
23. Milligan, J. F., and Uhlenbeck, O. C. (1989) Synthesis of small RNAs using T7 RNA polymerase, *Methods Enzymol. 180*, 51−62.
24. Chowrira, B. M., Berzal-Herranz, A., and Burke, J. M. (1993) Novel RNA polymerization reaction catalyzed by a group I ribozyme, *EMBO J. 12*, 3599−3605.
25. England, T. E., Bruce, A. G., and Uhlenbeck, O. C. (1980) Specific labeling of 3′ termini of RNA with T4 RNA ligase, *Methods Enzymol. 65*, 65−74.
26. Hampel, K. J., Pinard, R., and Burke, J. M. (2001) Catalytic and structural assays for the hairpin ribozyme, *Methods Enzymol. 341*, 566−580.
27. Hampel, K. J., and Burke, J. M. (2003) Solvent protection of the hammerhead ribozyme in the ground state: Evidence for a cation-assisted conformational change leading to catalysis, *Biochemistry 42*, 4421−4429.
28. Pinard, R., Heckman, J. E., and Burke, J. M. (1999) Alignment of the two domains of the hairpin ribozyme-substrate complex defined by interdomain photoaffinity crosslinking, *J. Mol. Biol. 287*, 239−251.
29. Sargueil, B., Hampel, K. J., Lambert, D., and Burke, J. M. (2003) In vitro selection of second site revertants analysis of the hairpin ribozyme active site, *J. Biol. Chem. 278*, 52783−52791.
30. Tullius, T. D., and Dombroski, B. A. (1985) Iron(II) EDTA used to measure the helical twist along any DNA molecule, *Science 230*, 679−681.
31. Tullius, T. D., Dombroski, B. A., Churchill, M. E., and Kam, L. (1987) Hydroxyl radical footprinting: A high-resolution method for mapping protein-DNA contacts, *Methods Enzymol. 155*, 537−558.
32. Balasubramanian, B., Pogozelski, W. K., and Tullius, T. D. (1998) DNA strand breaking by the hydroxyl radical is governed by the accessible surface areas of the hydrogen atoms of the DNA backbone, *Proc. Natl. Acad. Sci. U.S.A. 95*, 9738−9743.
33. Celander, D. W., and Cech, T. R. (1990) Iron(II)-ethylenediaminetetraacetic acid-catalyzed cleavage of RNA and DNA oligonucleotides: Similar reactivity toward single- and double-stranded forms, *Biochemistry 29*, 1355−1361.
34. Harris, M. E., Nolan, J. M., Malhotra, A., Brown, J. W., Harvey, S. C., and Pace, N. R. (1994) Use of photoaffinity crosslinking and molecular modeling to analyze the global architecture of ribonuclease P RNA, *EMBO J. 13*, 3953−3963.
35. Bravo, C., Lescure, F., Laugaa, P., Fourrey, J. L., and Favre, A. (1996) Folding of the HDV antigenomic ribozyme pseudoknot structure deduced from long-range photocrosslinks, *Nucleic Acids Res. 24*, 1351−1359.
36. Hampel, K. J., and Burke, J. M. (2001) A conformational change in the "loop E-like" motif of the hairpin ribozyme is coincidental with domain docking and is essential for catalysis, *Biochemistry 40*, 3723−3729.
37. Hiley, S. L., Sood, V. D., Fan, J., and Collins, R. A. (2002) 4-Thio-U cross-linking identifies the active site of the VS ribozyme, *EMBO J. 21*, 4691−4698.
38. Heckman, J. E., Lambert, D., and Burke, J. M. (2005) Photocrosslinking detects a compact, active structure of the hammerhead ribozyme, *Biochemistry 44*, 4148−4156.
39. Burgin, A. B., and Pace, N. R. (1990) Mapping the active site of ribonuclease P RNA using a substrate containing a photoaffinity agent, *EMBO J. 9*, 4111−4118.
40. Atmadja, J., Brimacombe, R., Blocker, H., and Frank, R. (1985) Investigation of the tertiary folding of *Escherichia coli* 16S RNA by in situ intra-RNA cross-linking within 30S ribosomal subunits, *Nucleic Acids Res. 13*, 6919−6936.
41. Cohen, S. B., and Cech, T. R. (1997) Dynamics of thermal motions within a large catalytic RNA investigated by cross-linking with thiol-disulfide interchange, *J. Am. Chem. Soc. 119*, 6259−6268.
42. Sclavi, B., Sullivan, M., Chance, M. R., Brenowitz, M., and Woodson, S. A. (1998) RNA folding at millisecond intervals by synchrotron hydroxyl radical footprinting, *Science 279*, 1940−1943.
43. Han, J., and Burke, J. M. (2005) Model for general acid-base catalysis by the hammerhead ribozyme: pH-activity relationships of G8 and G12 variants at the putative active site, *Biochemistry 44*, 7864−7870.
44. Keiper, S., Bebenroth, D., Seelig, B., Westhof, E., and Jaschke, A. (2004) Architecture of a Diels−Alderase ribozyme with a preformed catalytic pocket, *Chem. Biol. 11*, 1217−1227.
45. Serganov, A., Keiper, S., Malinina, L., Tereshko, V., Skripkin, E., Hobartner, C., Polonskaia, A., Phan, A. T., Wombacher, R., Micura, R., Dauter, Z., Jaschke, A., and Patel, D. J. (2005) Structural basis for Diels−Alder ribozyme-catalyzed carbon−carbon bond formation, *Nat. Struct. Mol. Biol. 12*, 218−224.
46. Frankel, A. D., and Smith, C. A. (1998) Induced folding in RNA-protein recognition: More than a simple molecular handshake, *Cell 92*, 149−151.
47. Williamson, J. R. (2000) Induced fit in RNA-protein recognition, *Nat. Struct. Biol. 7*, 834−837.
48. Serganov, A., Yuan, Y. R., Pikovskaya, O., Polonskaia, A., Malinina, L., Phan, A. T., Hobartner, C., Micura, R., Breaker, R. R., and Patel, D. J. (2004) Structural basis for discriminative regulation of gene expression by adenine- and guanine-sensing mRNAs, *Chem. Biol. 11*, 1729−1741.
49. Batey, R. T., Gilbert, S. D., and Montange, R. K. (2004) Structure of a natural guanine-responsive riboswitch complexed with the metabolite hypoxanthine, *Nature 432*, 411−415.
50. Feigon, J., Dieckmann, T., and Smith, F. W. (1996) Aptamer structures from A to zeta, *Chem. Biol. 3*, 611−617.

51. Tereshko, V., Skripkin, E., and Patel, D. J. (2003) Encapsulating streptomycin within a small 40-mer RNA, *Chem. Biol. 10*, 175−187.
52. Patel, D. J. (1997) Structural analysis of nucleic acid aptamers, *Curr. Opin. Chem. Biol. 1*, 32−46.
53. Rupert, P. B., and Ferre-D'Amare, A. R. (2001) Crystal structure of a hairpin ribozyme-inhibitor complex with implications for catalysis, *Nature 410*, 780−786.
54. Jaeger, L., Michel, F., and Westhof, E. (1994) Involvement of a GNRA tetraloop in long-range RNA tertiary interactions, *J. Mol. Biol. 236*, 1271−1276.
55. Costa, M., and Michel, F. (1997) Rules for RNA recognition of GNRA tetraloops deduced by in vitro selection: Comparison with in vivo evolution, *EMBO J. 16*, 3289−3302.

BI060337Z